Appendix B

Comparison of experimental data with the analytical model and numerical simulations of the cavity depth and cavity diameter upon drop impingement onto a steady liquid film

This appendix shows the evolution of the experimentally obtained results of the cavity depth and the cavity diameter, measured at $y_{cav}/h^* = 0.5$, with time. In each graph the analytical solution, given by eq. (4.3), and the numerical simulations are shown as well.

B.1 Evolution of the depth of the cavity in time

B.1.1 Influence of initial film thickness

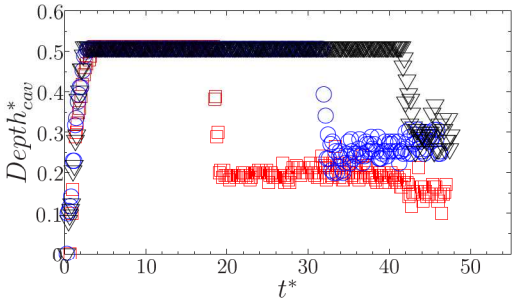

(a) Isopropanol; □: $h^* = 0.5$, $We = 194$, $Re = 1,208$; ◯: $h^* = 0.5$, $We = 384$, $Re = 1,701$; ▽: $h^* = 0.5$, $We = 541$, $Re = 2,007$

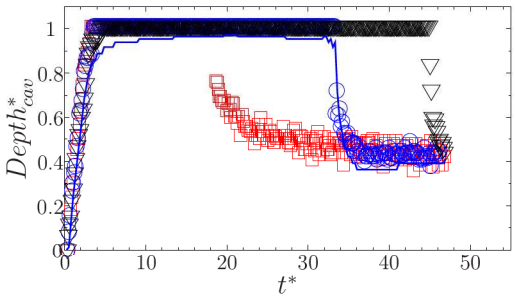

(b) Isopropanol; □: $h^* = 1.0$, $We = 192$, $Re = 1,201$; ◯: $h^* = 1.0$, $We = 384$, $Re = 1,701$; ▽: $h^* = 1.0$, $We = 539$, $Re = 2,013$

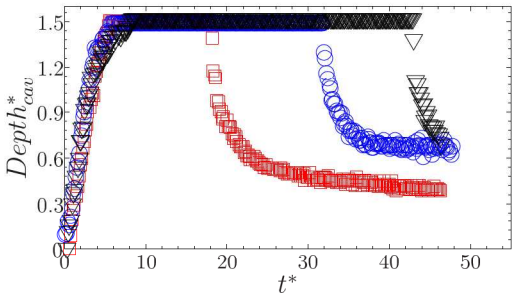

(c) Isopropanol; □: $h^* = 1.5$, $We = 192$, $Re = 1,206$; ◯: $h^* = 1.5$, $We = 392$, $Re = 1,733$; ▽: $h^* = 1.5$, $We = 535$, $Re = 2,006$

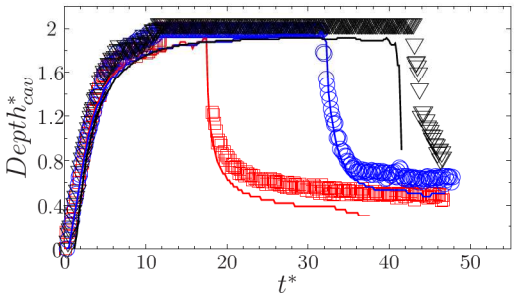

(d) Isopropanol; □: $h^* = 2.0$, $We = 189$, $Re = 1,199$; ◯: $h^* = 2.0$, $We = 392$, $Re = 1,733$; ▽: $h^* = 2.0$, $We = 527$, $Re = 1,982$

Figure B.1: Evolution of the depth of the cavity in time for different initial film thicknesses. Comparison of the experimental results (□, ◯, ▽) with the numerical simulations (solid line) for isopropanol. The impingement parameters for the experimental data and the inputs for the analytical model are listed in Table 4.2

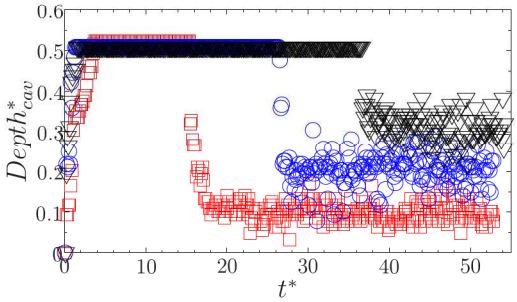

(a) Glycerine/water; □: $h^* = 0.5$, $We = 151$, $Re = 299$; ◯: $h^* = 0.5$, $We = 318$, $Re = 444$; ▽: $h^* = 0.5$, $We = 472$, $Re = 539$

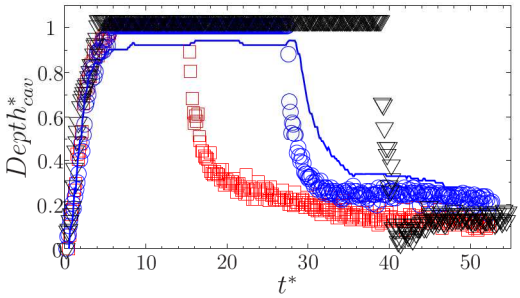

(b) Glycerine/water; □: $h^* = 1.0$, $We = 162$, $Re = 341$; ◯: $h^* = 1.0$, $We = 329$, $Re = 428$; ▽: $h^* = 1.0$, $We = 465$, $Re = 526$

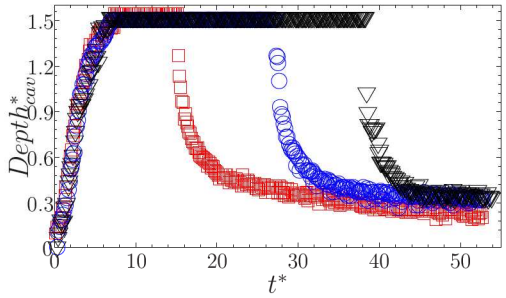

(c) Glycerine/water; □: $h^* = 1.5$, $We = 156$, $Re = 317$; ◯: $h^* = 1.5$, $We = 328$, $Re = 447$; ▽: $h^* = 1.5$, $We = 473$, $Re = 529$

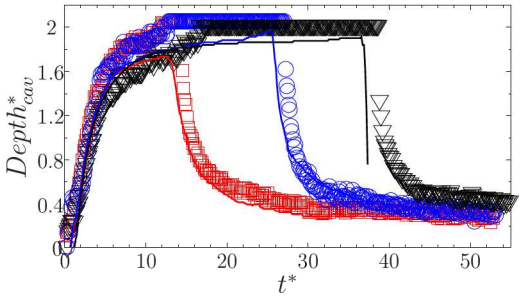

(d) Glycerine/water; □: $h^* = 2.0$, $We = 157$, $Re = 320$; ◯: $h^* = 2.0$, $We = 308$, $Re = 434$; ▽: $h^* = 2.0$, $We = 505$, $Re = 561$

Figure B.2: Evolution of the depth of the cavity in time for different initial film thicknesses. Comparison of the experimental results (□, ◯, ▽) with the numerical simulations (solid line) for glycerine/water mixture. The impingement parameters for the experimental data and the inputs for the analytical model are listed in Table 4.2

B.1.2 Influence of impingement Weber number

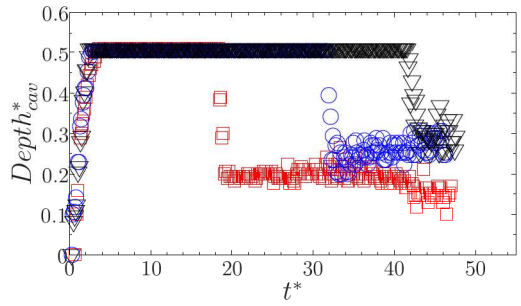

(a) Isopropanol; □: $h^* = 0.5$, $We = 194$, $Re = 1,208$; ◯: $h^* = 0.5$, $We = 384$, $Re = 1,701$; ▽: $h^* = 0.5$, $We = 541$, $Re = 2,006$

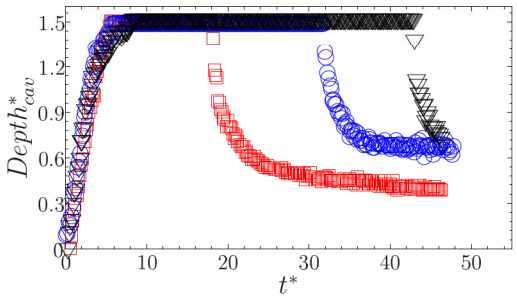

(b) Isopropanol; □: $h^* = 1.5$, $We = 192$, $Re = 1,206$; ◯: $h^* = 1.5$, $We = 392$, $Re = 1,733$; ▽: $h^* = 1.5$, $We = 535$, $Re = 2,006$

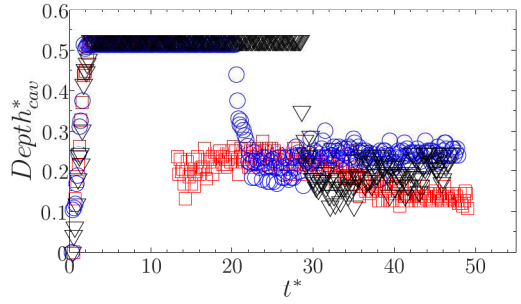

(c) Distilled water; □: $h^* = 0.5$, $We = 111$, $Re = 4,871$; ◯: $h^* = 0.5$, $We = 238$, $Re = 7,173$; ▽: $h^* = 0.5$, $We = 332$, $Re = 8,392$

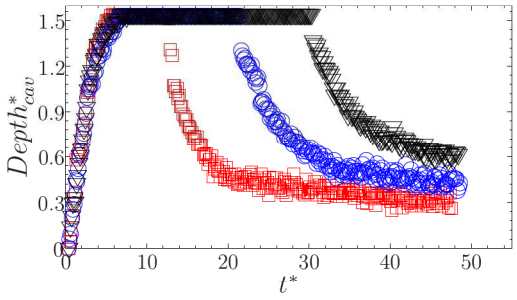

(d) Distilled water; □: $h^* = 1.5$, $We = 110$, $Re = 4,870$; ◯: $h^* = 1.5$, $We = 232$, $Re = 7,115$; ▽: $h^* = 1.5$, $We = 341$, $Re = 8,587$

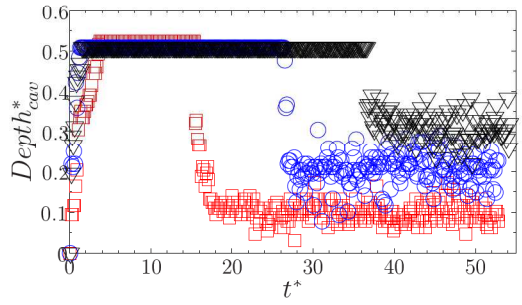

(e) Glycerine/water; □: $h^* = 0.5$, $We = 151$, $Re = 299$; ◯: $h^* = 0.5$, $We = 308$, $Re = 444$; ▽: $h^* = 0.5$, $We = 472$, $Re = 539$

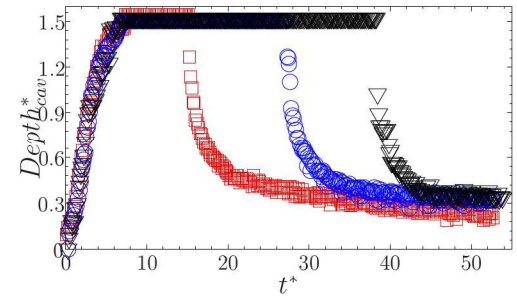

(f) Glycerine/water; □: $h^* = 1.5$, $We = 156$, $Re = 317$; ◯: $h^* = 1.5$, $We = 328$, $Re = 447$; ▽: $h^* = 1.5$, $We = 473$, $Re = 529$

Figure B.3: Evolution of the depth of the cavity in time for an initial film thickness of $h^* = 0.5$ (left) and $h^* = 1.5$ (right). Comparison of the experimental results (□, ◯, ▽) with the numerical simulations (solid line) for (a)-(b) isopropanol, (c)-(d) distilled water and (e)-(f) glycerine/water. The impingement parameters for the experimental data and the inputs for the analytical model are listed in Table 4.2

B.1.3 Influence of liquid properties

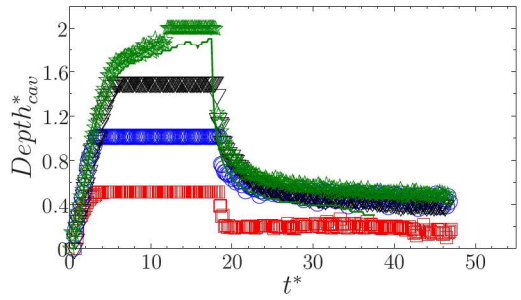

(a) Isopropanol; □: $h^* = 0.5$, $We = 194$, $Re = 1,208$; ◯: $h^* = 1.0$, $We = 192$, $Re = 1,201$; ▽: $h^* = 1.5$, $We = 192$, $Re = 1,206$; ★: $h^* = 2.0$, $We = 189$, $Re = 1,199$

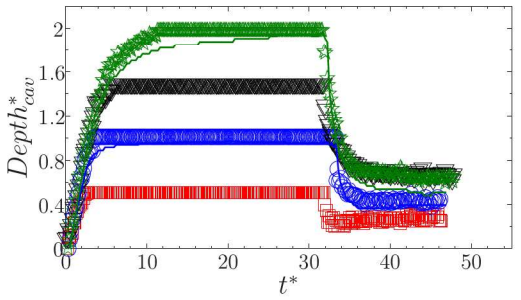

(b) Isopropanol; □: $h^* = 0.5$, $We = 384$, $Re = 1,701$; ◯: $h^* = 1.0$, $We = 384$, $Re = 1,701$; ▽: $h^* = 1.5$, $We = 392$, $Re = 1,733$; ★: $h^* = 2.0$, $We = 392$, $Re = 1,733$

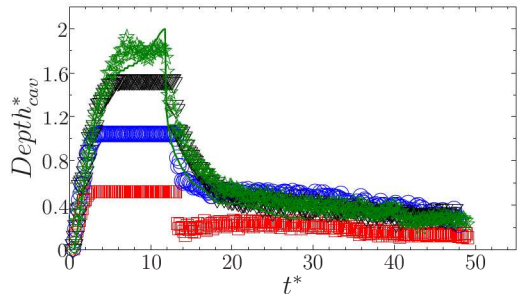

(c) Distilled water; □: $h^* = 0.5$, $We = 111$, $Re = 4,871$; ◯: $h^* = 1.0$, $We = 105$, $Re = 4,744$; ▽: $h^* = 1.5$, $We = 110$, $Re = 4,870$; ★: $h^* = 2.0$, $We = 113$, $Re = 4,948$

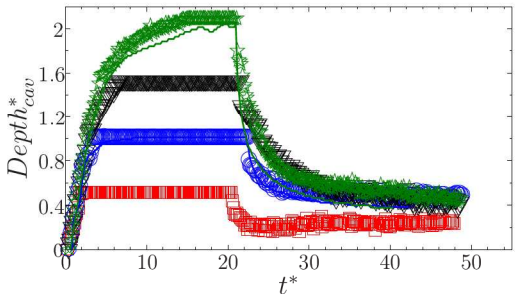

(d) Distilled water; □: $h^* = 0.5$, $We = 238$, $Re = 7,173$; ◯: $h^* = 1.0$, $We = 239$, $Re = 7,241$; ▽: $h^* = 1.5$, $We = 232$, $Re = 7,115$; ★: $h^* = 2.0$, $We = 215$, $Re = 6,750$

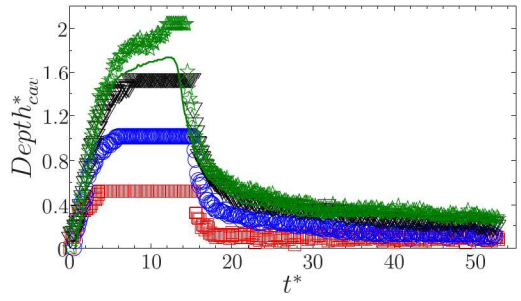

(e) Glycerine/water; □: $h^* = 0.5$, $We = 151$, $Re = 299$; ◯: $h^* = 1.0$, $We = 162$, $Re = 341$; ▽: $h^* = 1.5$, $We = 156$, $Re = 317$; ★: $h^* = 2.0$, $We = 157$, $Re = 320$

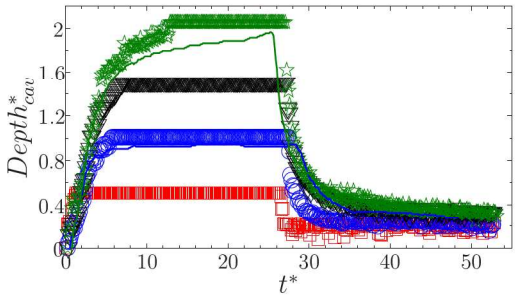

(f) Glycerine/water; □: $h^* = 0.5$, $We = 318$, $Re = 444$; ◯: $h^* = 1.0$, $We = 329$, $Re = 428$; ▽: $h^* = 1.5$, $We = 328$, $Re = 447$; ★: $h^* = 2.0$, $We = 308$, $Re = 434$

Figure B.4: Evolution of the depth of the cavity in time for the lowest (left) and medium (right) drop Weber numbers and four film thicknesses. Comparison of the experimental results (□, ◯, ▽, ★) with the numerical simulations (solid line) for (a)-(b) isopropanol, (c)-(d) distilled water and (e)-(f) glycerine/water. The impingement parameters for the experimental data and the inputs for the analytical model are listed in Table 4.2

B.2 Evolution of the diameter of the cavity in time

B.2.1 Influence of initial film thickness

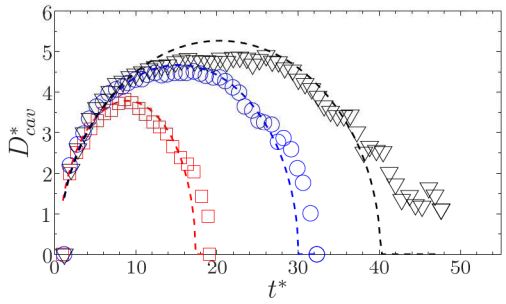

(a) Isopropanol; □: $h^* = 0.5$, $We = 194$, $Re = 1,208$; ◯: $h^* = 0.5$, $We = 384$, $Re = 1,701$; ▽: $h^* = 0.5$, $We = 541$, $Re = 2,007$

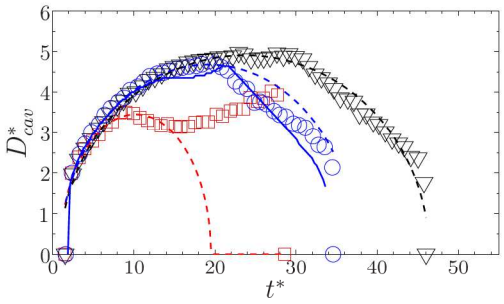

(b) Isopropanol; □: $h^* = 1.0$, $We = 192$, $Re = 1,201$; ◯: $h^* = 1.0$, $We = 384$, $Re = 1,701$; ▽: $h^* = 1.0$, $We = 539$, $Re = 2,013$

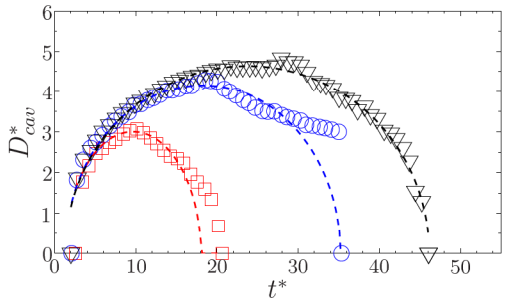

(c) Isopropanol; □: $h^* = 1.5$, $We = 192$, $Re = 1,206$; ◯: $h^* = 1.5$, $We = 392$, $Re = 1,733$; ▽: $h^* = 1.5$, $We = 535$, $Re = 2,006$

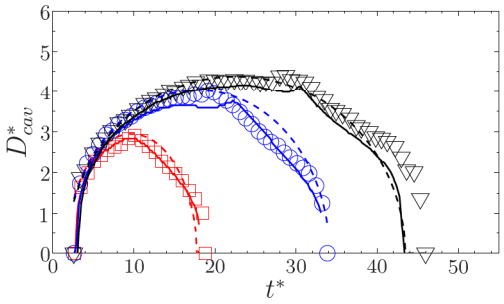

(d) Isopropanol; □: $h^* = 2.0$, $We = 189$, $Re = 1,199$; ◯: $h^* = 2.0$, $We = 392$, $Re = 1,733$; ▽: $h^* = 2.0$, $We = 527$, $Re = 1,982$

Figure B.5: Evolution of the diameter of the cavity in time, measured at $y/h^*_{cav} = 0.5$, for different initial film thicknesses. Comparison of the experimental results (□, ◯, ▽) with the theoretical predictions (eq. (4.10), dashed line) and the numerical simulations (solid line) for isopropanol. The impingement parameters for the experimental data and the inputs for the analytical model are listed in Table 4.2

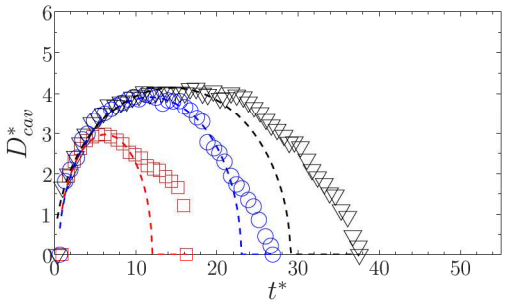

(a) Glycerine/water; □: $h^* = 0.5$, $We = 151$, $Re = 299$; ◯: $h^* = 0.5$, $We = 318$, $Re = 444$; ▽: $h^* = 0.5$, $We = 472$, $Re = 539$

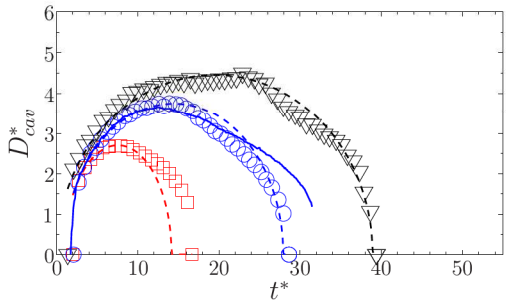

(b) Glycerine/water; □: $h^* = 1.0$, $We = 162$, $Re = 341$; ◯: $h^* = 1.0$, $We = 329$, $Re = 428$; ▽: $h^* = 1.0$, $We = 465$, $Re = 526$

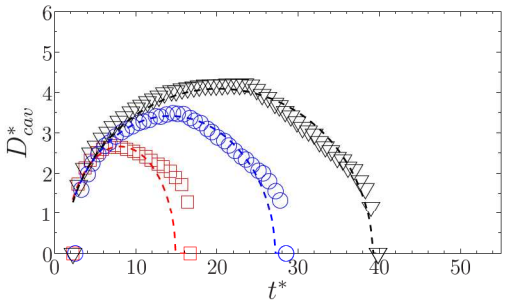

(c) Glycerine/water; □: $h^* = 1.5$, $We = 156$, $Re = 317$; ◯: $h^* = 1.5$, $We = 328$, $Re = 444$; ▽: $h^* = 1.5$, $We = 473$, $Re = 529$

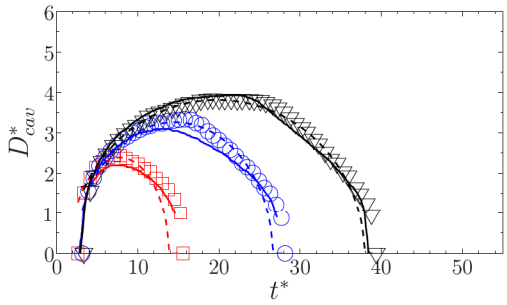

(d) Glycerine/water; □: $h^* = 2.0$, $We = 157$, $Re = 320$; ◯: $h^* = 2.0$, $We = 308$, $Re = 434$; ▽: $h^* = 2.0$, $We = 505$, $Re = 561$

Figure B.6: Evolution of the diameter of the cavity in time, measured at $y/h^*_{cav} = 0.5$, for different initial film thicknesses. Comparison of the experimental results (□, ◯, ▽) with the theoretical predictions (eq. (4.10), dashed line) and the numerical simulations (solid line) for glycerine/water mixture. The impingement parameters for the experimental data and the inputs for the analytical model are listed in Table 4.2

B.2.2 Influence of impingement Weber number

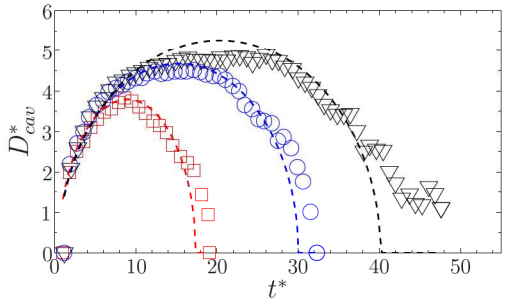

(a) Isopropanol; □: $h^* = 0.5$, $We = 194$, $Re = 1,208$; ◯: $h^* = 0.5$, $We = 384$, $Re = 1,701$; ▽: $h^* = 0.5$, $We = 541$, $Re = 2,007$

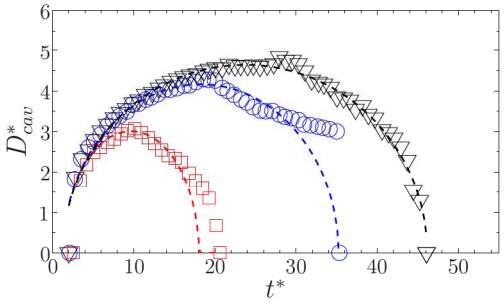

(b) Isopropanol; □: $h^* = 1.5$, $We = 192$, $Re = 1,206$; ◯: $h^* = 1.5$, $We = 392$, $Re = 1,733$; ▽: $h^* = 1.5$, $We = 535$, $Re = 2,006$

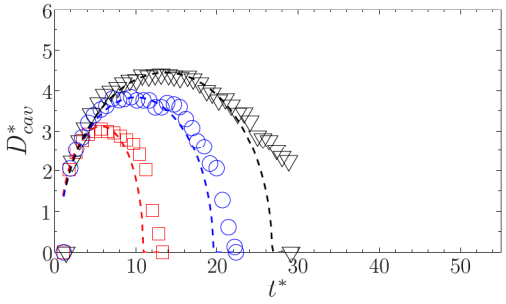

(c) Distilled water; □: $h^* = 0.5$, $We = 111$, $Re = 4,871$; ◯: $h^* = 0.5$, $We = 238$, $Re = 7,173$; ▽: $h^* = 0.5$, $We = 332$, $Re = 8,392$

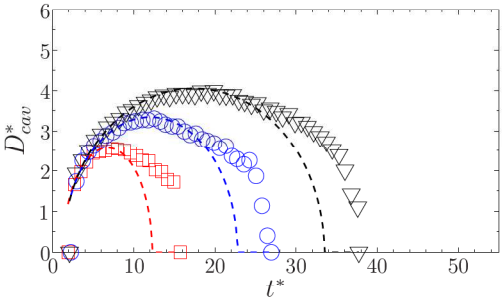

(d) Distilled water; □: $h^* = 1.5$, $We = 110$, $Re = 4,870$; ◯: $h^* = 1.5$, $We = 232$, $Re = 7,115$; ▽: $h^* = 1.5$, $We = 341$, $Re = 8,587$

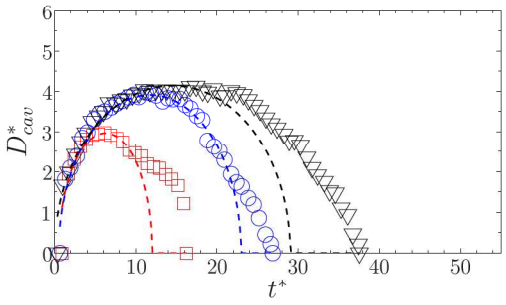

(e) Glycerine/water; □: $h^* = 0.5$, $We = 151$, $Re = 299$; ◯: $h^* = 0.5$, $We = 318$, $Re = 444$; ▽: $h^* = 0.5$, $We = 472$, $Re = 539$

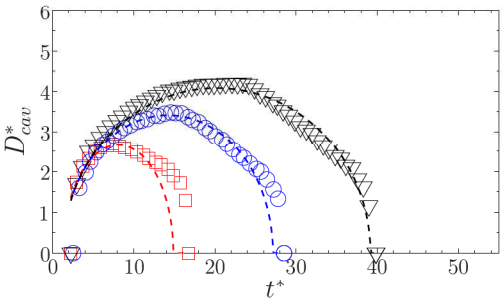

(f) Glycerine/water; □: $h^* = 1.5$, $We = 156$, $Re = 317$; ◯: $h^* = 1.5$, $We = 328$, $Re = 260$; ▽: $h^* = 1.5$, $We = 473$, $Re = 529$

Figure B.7: Evolution of the diameter of the cavity in time, measured at $y/h^*_{cav} = 0.5$, for an initial film thickness of $h^* = 0.5$ (left) and $h^* = 1.5$ (right). Comparison of the experimental results (□, ◯, ▽) with the theoretical predictions (eq. (4.10), dashed line) and the numerical simulations (solid line) for (a)-(b) isopropanol, (c)-(d) distilled water and (e)-(f) glycerine/water. The impingement parameters for the experimental data and the inputs for the analytical model are listed in Table 4.2

B.2.3 Influence of liquid properties

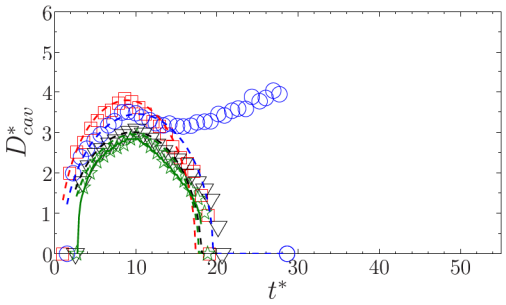

(a) Isopropanol; □: $h^* = 0.5$, $We = 194$, $Re = 1,208$; ◯: $h^* = 1.0$, $We = 192$, $Re = 1,701$; ▽: $h^* = 1.5$, $We = 192$, $Re = 1,206$; ★: $h^* = 2.0$, $We = 189$, $Re = 1,199$

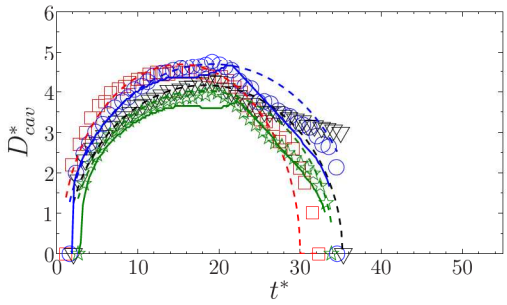

(b) Isopropanol; □: $h^* = 0.5$, $We = 384$, $Re = 1,701$; ◯: $h^* = 1.0$, $We = 384$, $Re = 1,701$; ▽: $h^* = 1.5$, $We = 392$, $Re = 1,733$; ★: $h^* = 2.0$, $We = 392$, $Re = 1,733$

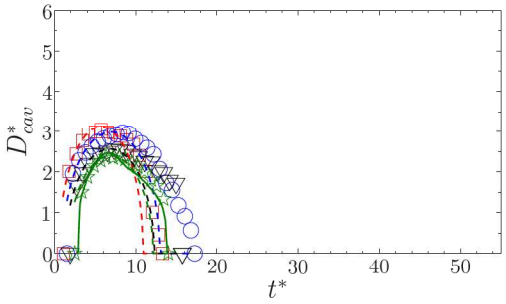

(c) Distilled water; □: $h^* = 0.5$, $We = 111$, $Re = 4,871$; ◯: $h^* = 1.0$, $We = 105$, $Re = 4,744$; ▽: $h^* = 1.5$, $We = 110$, $Re = 4,870$; ★: $h^* = 2.0$, $We = 113$, $Re = 4,948$

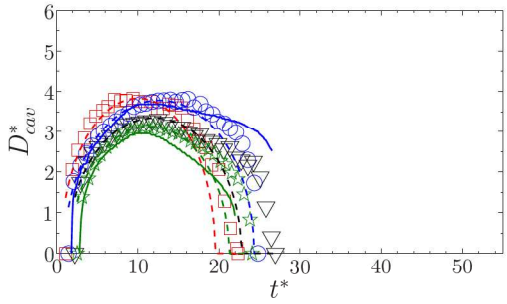

(d) Distilled water; □: $h^* = 0.5$, $We = 238$, $Re = 7,173$; ◯: $h^* = 1.0$, $We = 239$, $Re = 7,241$; ▽: $h^* = 1.5$, $We = 232$, $Re = 7,115$; ★: $h^* = 2.0$, $We = 215$, $Re = 6,750$

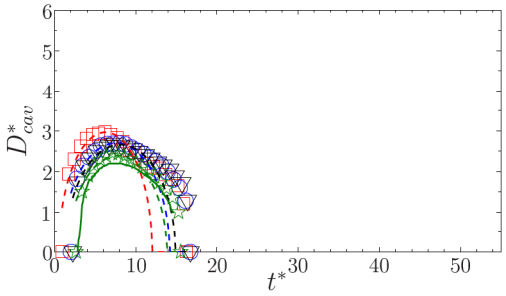

(e) Glycerine/water; □: $h^* = 0.5$, $We = 151$, $Re = 299$; ◯: $h^* = 1.0$, $We = 162$, $Re = 341$; ▽: $h^* = 1.5$, $We = 156$, $Re = 317$; ★: $h^* = 2.0$, $We = 157$, $Re = 320$

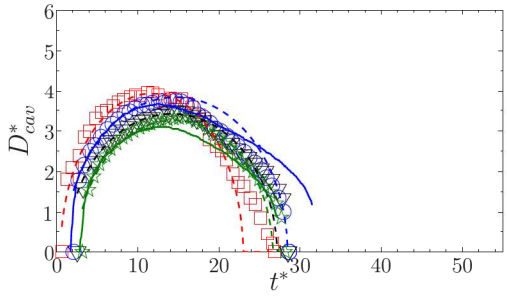

(f) Glycerine/water; □: $h^* = 0.5$, $We = 318$, $Re = 444$; ◯: $h^* = 1.0$, $We = 329$, $Re = 428$; ▽: $h^* = 1.5$, $We = 328$, $Re = 447$; ★: $h^* = 2.0$, $We = 308$, $Re = 434$

Figure B.8: Evolution of the diameter of the cavity in time, measured at $y/h^*_{cav} = 0.5$, for the lowest (left) and medium (right) drop Weber numbers and four film thicknesses. Comparison of the experimental results (□, ◯, ▽, ★) with the theoretical predictions (eq. (4.10), dashed line) and the numerical simulations (solid line) for (a)-(b) isopropanol, (c)-(d) distilled water and (e)-(f) glycerine/water. The impingement parameters for the experimental data and the inputs for the analytical model are listed in Table 4.2

Appendix C

Influence of the Weber number on the time evolution of the relative diameter of the cavity upon drop impingement onto a solitary surface wave

This appendix gives an overview of the evolution of the relative diameter of the cavity in time for different Weber numbers. A comparison is made of the experimental results for the single drop impingement onto different phases of the small and large waves at different Weber numbers of the drop upon impingement for both studied liquids.

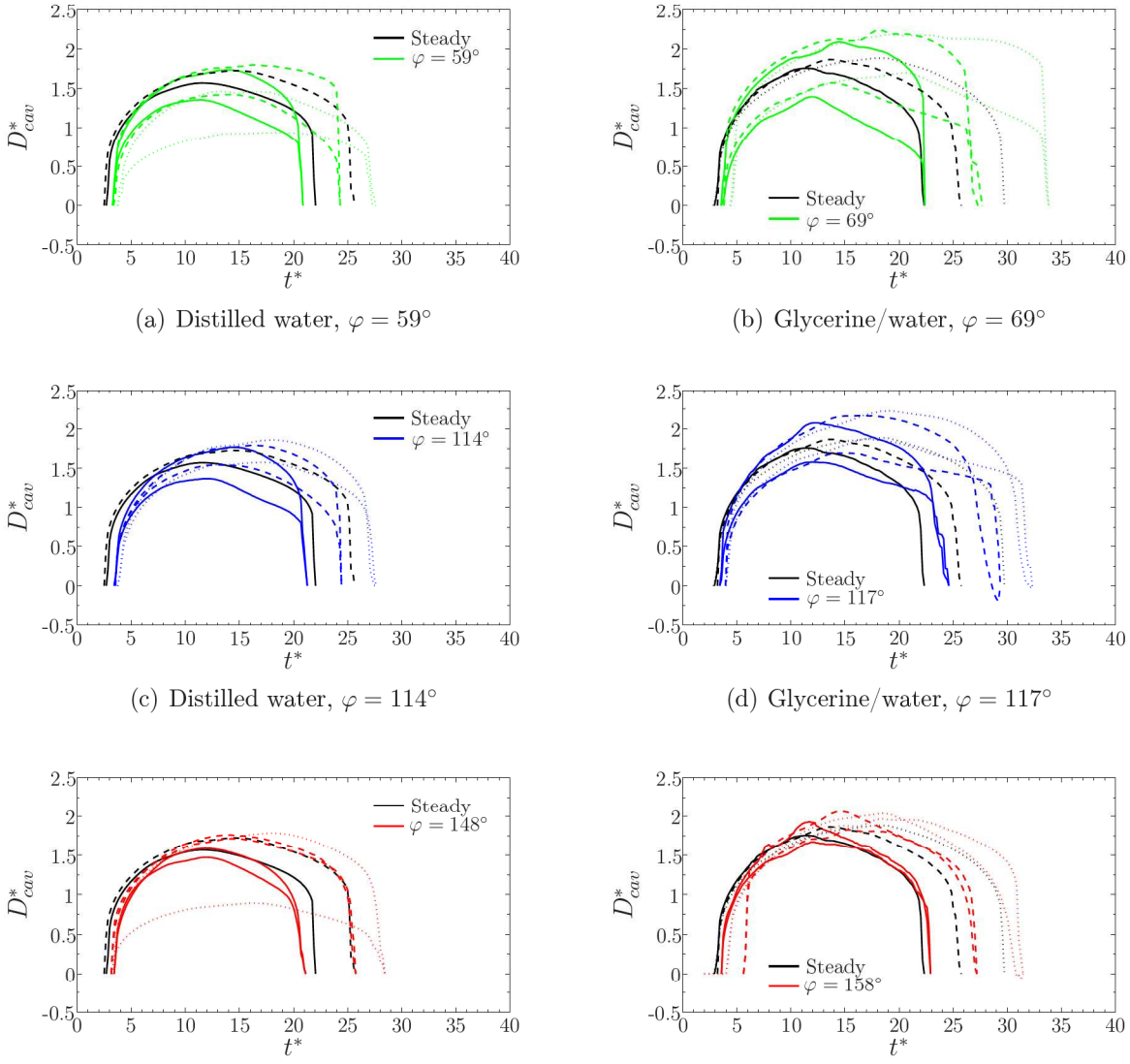

(a) Distilled water, $\varphi = 59°$

(b) Glycerine/water, $\varphi = 69°$

(c) Distilled water, $\varphi = 114°$

(d) Glycerine/water, $\varphi = 117°$

(e) Distilled water, $\varphi = 148°$

(f) Glycerine/water, $\varphi = 158°$

Figure C.1: Evolution of the relative diameter of the cavity in time for different Weber numbers. Comparison of the experimental results for the single drop impingement onto different phases of the small solitary wave. The impingement parameters are for distilled water $We = 304$, $Re = 10,411$ (solid line), $We = 378$, $Re = 11,611$ (dashed line) and $We = 398$, $Re = 11,458$ (dotted line); for glycerine/water: $We = 185$, $Re = 7,276$ (solid line), $We = 232$, $Re = 8,191$ (dashed line) and $We = 284$, $Re = 8,980$ (dotted line)

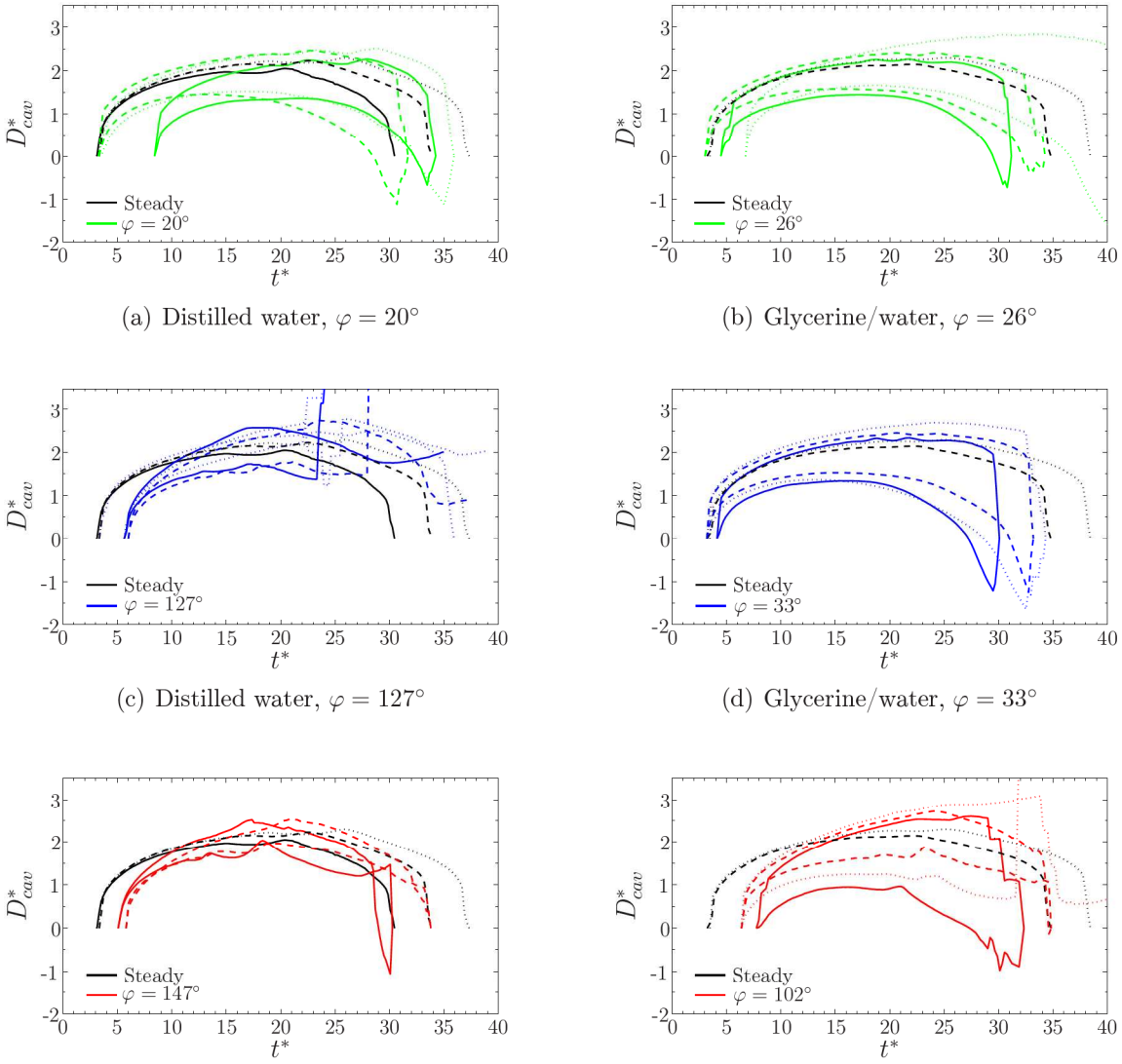

(a) Distilled water, $\varphi = 20°$

(b) Glycerine/water, $\varphi = 26°$

(c) Distilled water, $\varphi = 127°$

(d) Glycerine/water, $\varphi = 33°$

(e) Distilled water, $\varphi = 147°$

(f) Glycerine/water, $\varphi = 102°$

Figure C.2: Evolution of the relative diameter of the cavity in time for different Weber numbers. Comparison of the experimental results for the single drop impingement onto different phases of the large solitary wave. The impingement parameters are for distilled water $We = 285$, $Re = 9,170$ (solid line), $We = 346$, $Re = 10,169$ (dashed line) and $We = 389$, $Re = 10,796$ (dotted line); for glycerine/water: $We = 282$, $Re = 9.004$ (solid line), $We = 337$, $Re = 9,873$ (dashed line) and $We = 361$, $Re = 10,112$ (dotted line)

Appendix D

In-plane surface film velocity fluctuations by spray impingement

In this appendix the results are shown of the velocity fluctuations in both in-plane directions inside the surface film that appears for spray impingement onto a solid target. The results are shown for both investigated ultrasonic nozzles, US10 and US20, applied with and without carrier gas, and for different volume flows between 100 mL/min and 200 mL/min for US10 and between 100 mL/min and 300 mL/min for US20. For each nozzle, two spray impingement heights are investigated, hence 48.8 mm and 110 mm for US10 and 61.3 mm and 122.5 mm for US20.

D.1 Distributions of the velocity fluctuations in x-direction

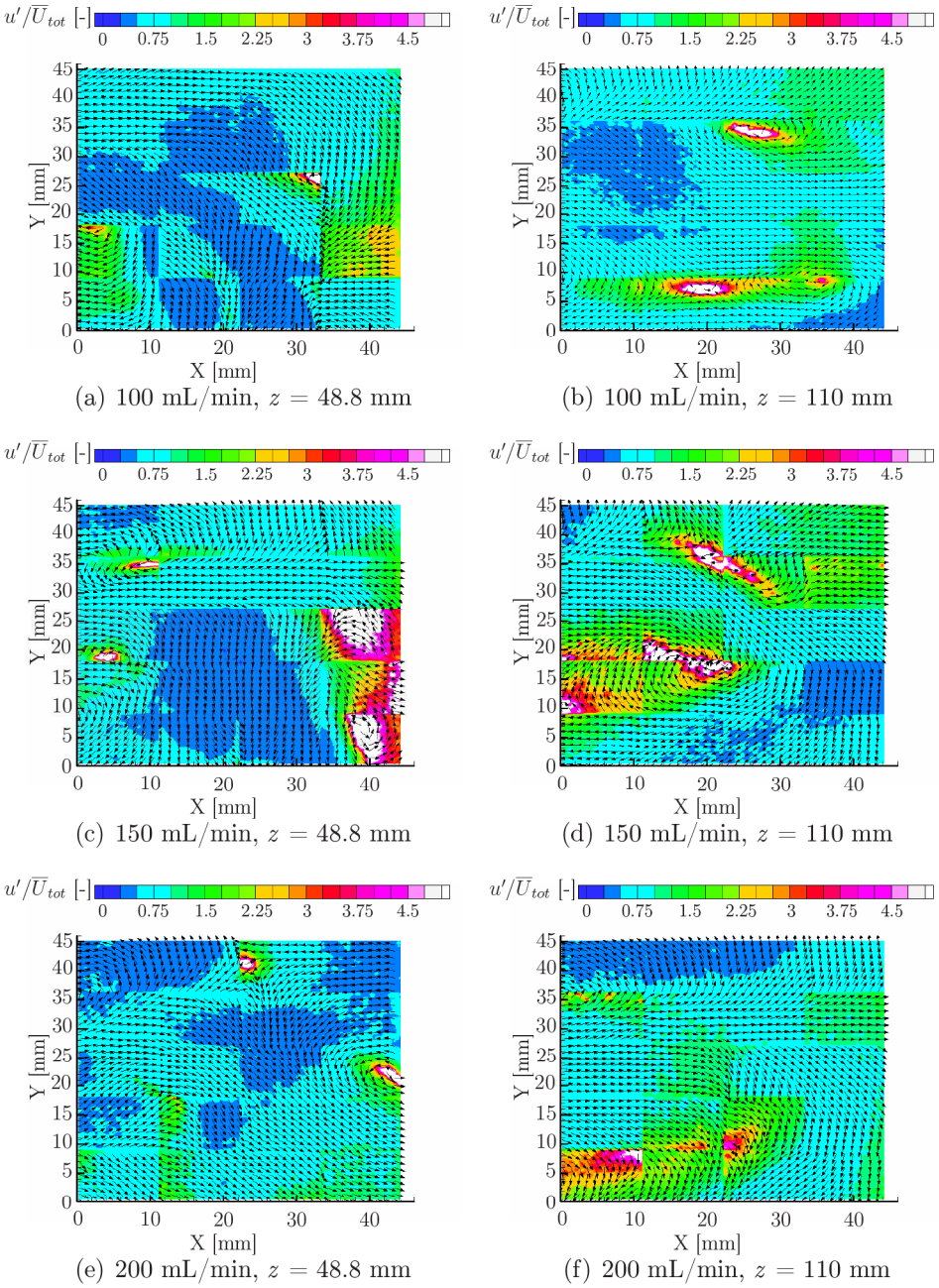

(a) 100 mL/min, $z = 48.8$ mm (b) 100 mL/min, $z = 110$ mm

(c) 150 mL/min, $z = 48.8$ mm (d) 150 mL/min, $z = 110$ mm

(e) 200 mL/min, $z = 48.8$ mm (f) 200 mL/min, $z = 110$ mm

Figure D.1: Distributions of the horizontal velocity fluctuations ($u'/\overline{U}_{tot}$) inside the surface film for impingement of a spray, generated by the ultrasonic US10 nozzle, applied with pressurized air at 0.604 bar, for different volume flows between 100 mL/min and 200 mL/min at the axial positions $z = 48.8$ mm (left) and $z = 110$ mm (right)

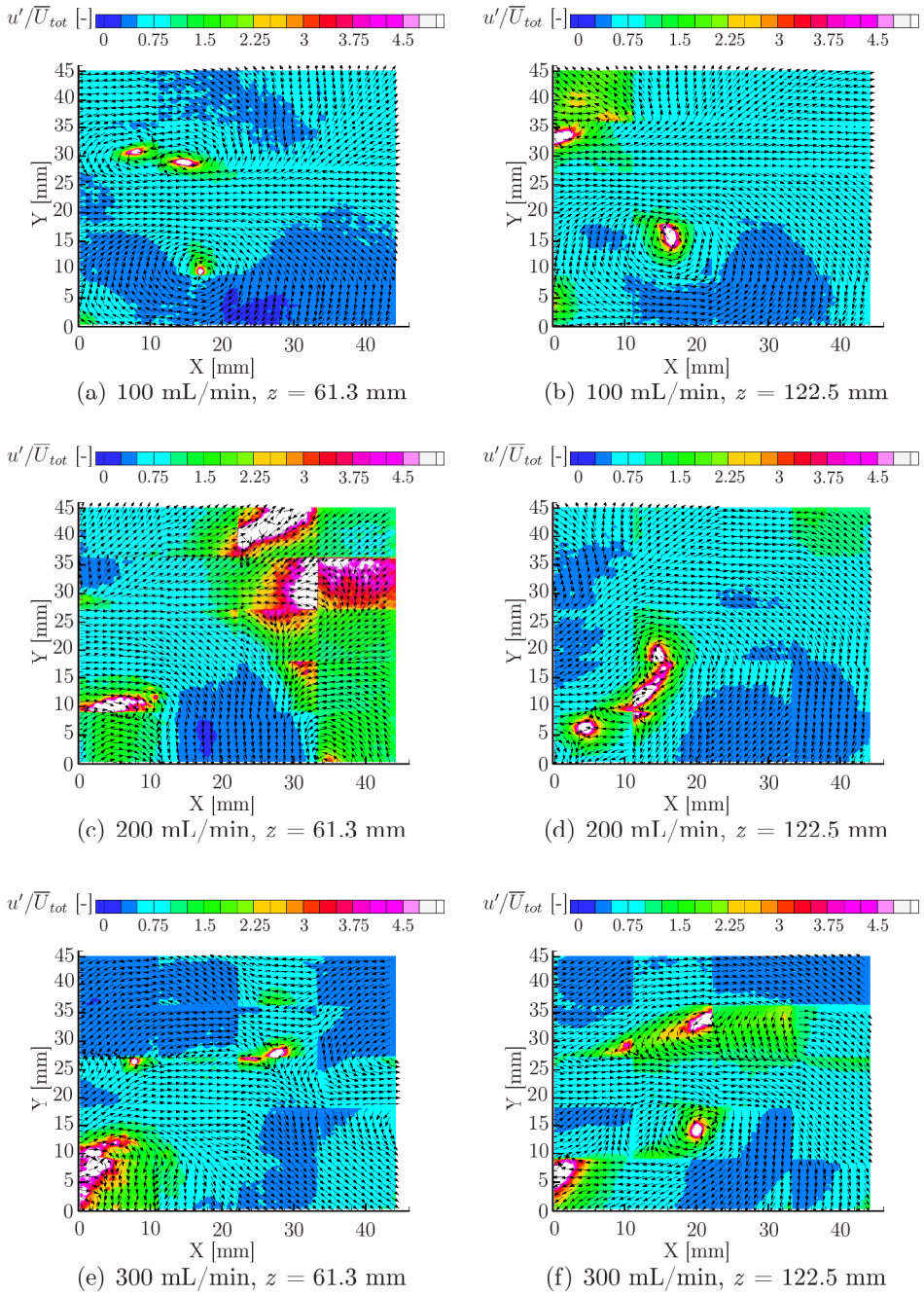

(a) 100 mL/min, $z = 61.3$ mm

(b) 100 mL/min, $z = 122.5$ mm

(c) 200 mL/min, $z = 61.3$ mm

(d) 200 mL/min, $z = 122.5$ mm

(e) 300 mL/min, $z = 61.3$ mm

(f) 300 mL/min, $z = 122.5$ mm

Figure D.2: Distributions of the horizontal velocity fluctuations ($u'/\overline{U}_{tot}$) inside the surface film for impingement of a spray, generated by the ultrasonic US20 nozzle, applied with pressurized air at 0.604 bar, for different volume flows between 100 mL/min and 300 mL/min at the axial positions $z = 61.3$ mm (left) and $z = 122.5$ mm (right)

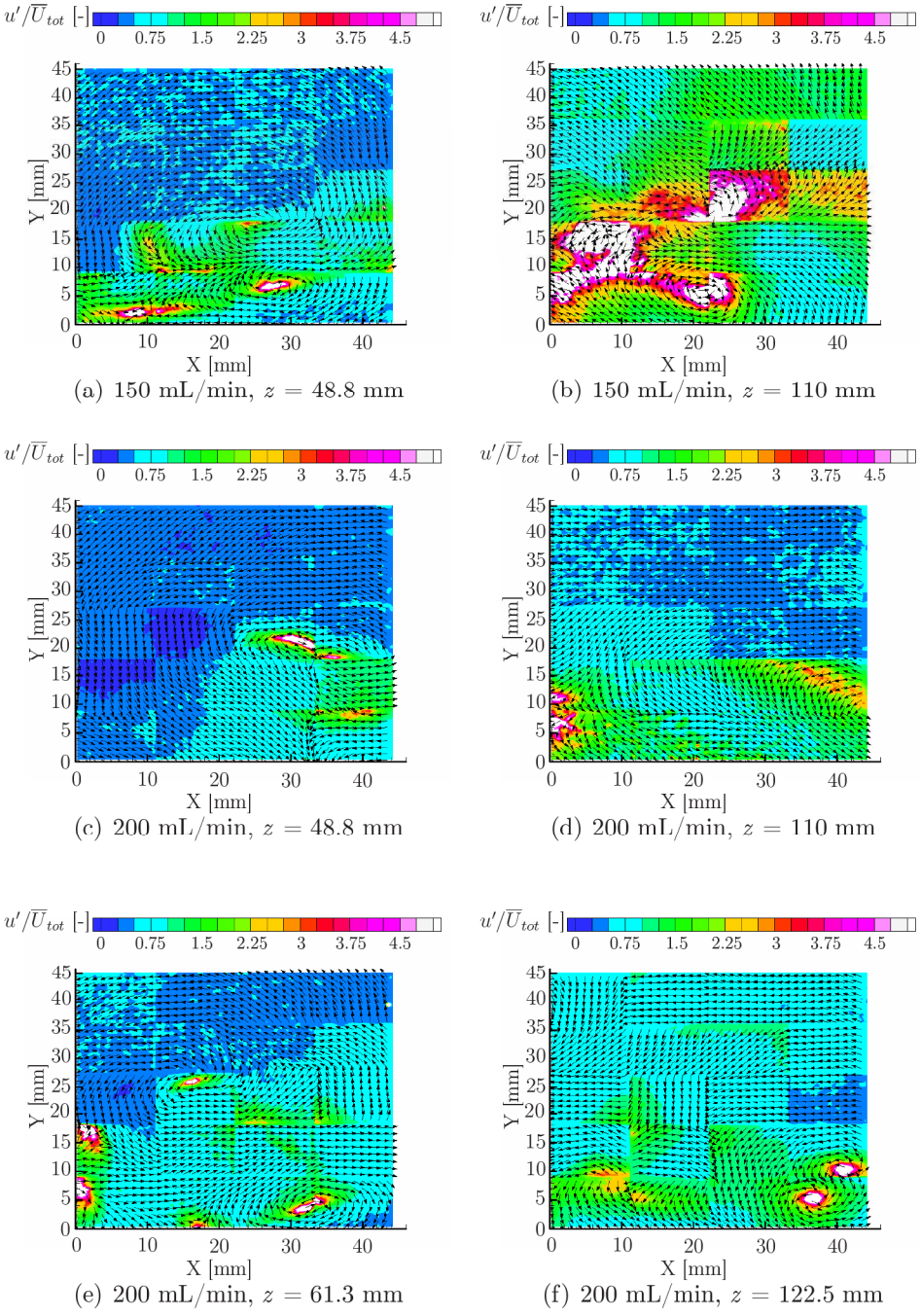

(a) 150 mL/min, z = 48.8 mm

(b) 150 mL/min, z = 110 mm

(c) 200 mL/min, z = 48.8 mm

(d) 200 mL/min, z = 110 mm

(e) 200 mL/min, z = 61.3 mm

(f) 200 mL/min, z = 122.5 mm

Figure D.3: Distributions of the horizontal velocity fluctuations ($u'/\overline{U}_{tot}$) inside the surface film for impingement of a spray, generated by the ultrasonic US10 (a-d) and US20 (e-f) nozzles, without carrier gas, for two different volume flows of 150 mL/min and 200 mL/min at the axial positions z = 48.8 mm (left) and z = 110 mm (right) for US10 and at z = 61.3 mm (left) and z = 122.5 mm (right) for US20

D.2 Distributions of the velocity fluctuations in y-direction

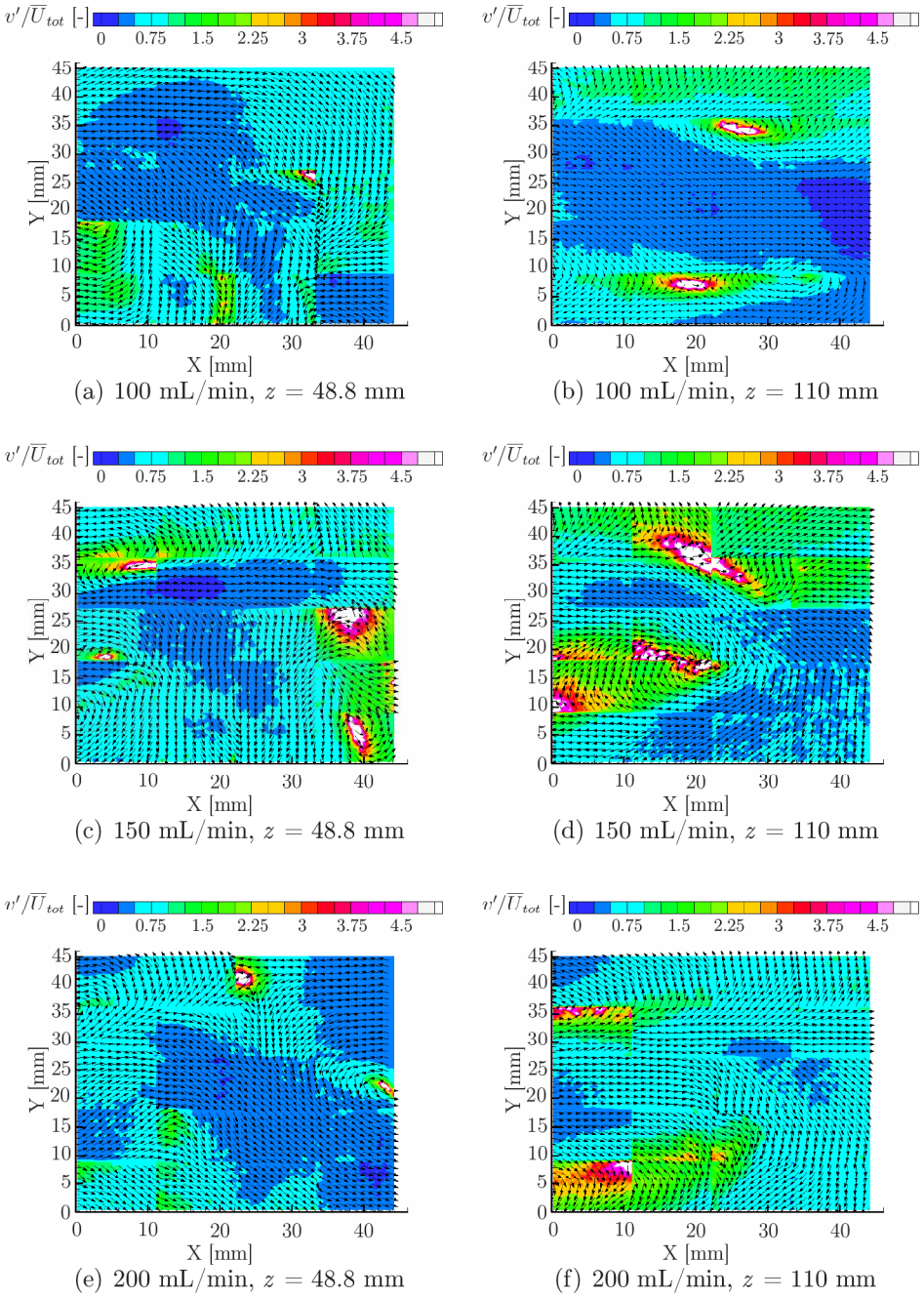

(a) 100 mL/min, $z = 48.8$ mm (b) 100 mL/min, $z = 110$ mm

(c) 150 mL/min, $z = 48.8$ mm (d) 150 mL/min, $z = 110$ mm

(e) 200 mL/min, $z = 48.8$ mm (f) 200 mL/min, $z = 110$ mm

Figure D.4: Distributions of the vertical velocity fluctuations ($v'/\overline{U}_{tot}$) inside the surface film for impingement of a spray, generated by the ultrasonic US10 nozzle, applied with pressurized air at 0.604 bar, for different volume flows between 100 mL/min and 200 mL/min at the axial positions $z = 48.8$ mm (left) and $z = 110$ mm (right)

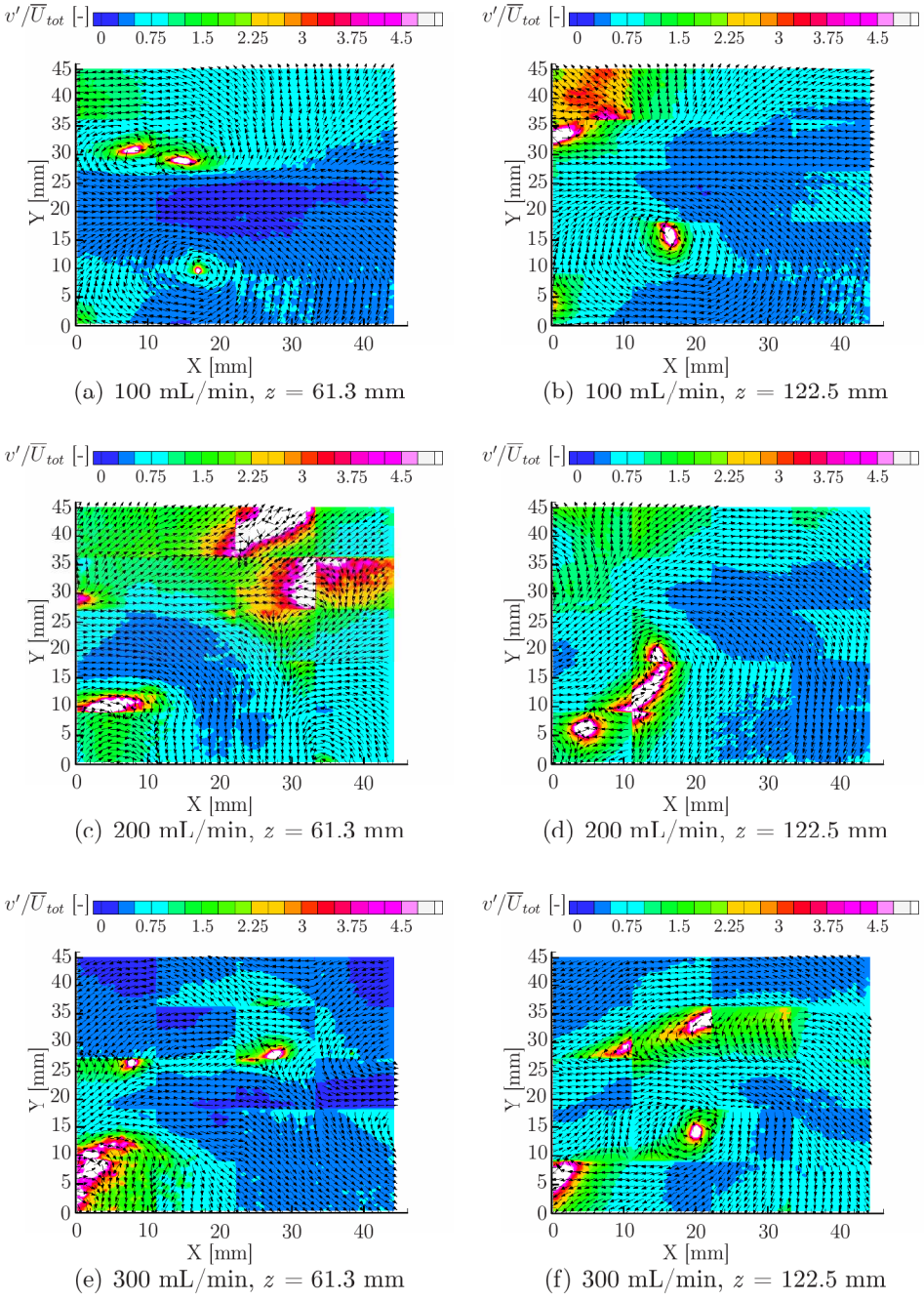

(a) 100 mL/min, $z = 61.3$ mm

(b) 100 mL/min, $z = 122.5$ mm

(c) 200 mL/min, $z = 61.3$ mm

(d) 200 mL/min, $z = 122.5$ mm

(e) 300 mL/min, $z = 61.3$ mm

(f) 300 mL/min, $z = 122.5$ mm

Figure D.5: Distributions of the vertical velocity fluctuations ($v'/\overline{U}_{tot}$) inside the surface film for impingement of a spray, generated by the ultrasonic US20 nozzle, applied with pressurized air at 0.604 bar, for different volume flows between 100 mL/min and 300 mL/min at the axial positions $z = 61.3$ mm (left) and $z = 122.5$ mm (right)